A Novel Coupler Design and Analysis with Shielding Material Tests for a CPT System of Electric Vehicles Based on Electromagnetic Resonant Coupling

IOP Conf. Series: Materials Science and Engineering **647** (2019) 012005 doi:10.1088/1757-899X/647/1/012005

A Novel Coupler Design and Analysis with Shielding Material Tests for a CPT System of Electric Vehicles Based on Electromagnetic Resonant Coupling

J Duan[1,*] and W Wang[2]

[1,2] Department of Engineering and Design, University of Sussex, Brighton BN1 9QT, United Kingdom

* J.Duan@sussex.ac.uk.

Abstract. In this paper, a contactless power transfer (CPT) system using a novel geometrically enhanced energy transfer coupler with three different shielding materials has been built and analysed, along with the evaluations from aspects of electromagnetics and RMS power transmitting based on electromagnetic resonant coupling. A CPT system design improvement with the proposed H-shape ferromagnetic cores and the combined semi-enclosed passive electromagnetic shielding methods have been investigated in terms of generated electromagnetic field characteristics, system power transfer ratings, system efficiency optimization and performances of shielding materials. The results have shown that, across the range of operating frequency of the CPT system, aluminium shielding as a metallic material method could deliver better overall CPT system performance than other two ferromagnetic materials, steel 1010 and ferrite. In addition, the coupler prototype design limitations, misalignment tolerance and the passive shielding design considerations including distance between windings and inner surfaces of shielding shells have been discussed.

1. Introduction

Contactless power transfer (CPT) technologies based on inductive coupling have been developed to a series of applications in daily and industrial areas, such as small electronic devices, dynamic automotive battery systems, public transportations, medical implants, instrumentation test systems, and so on [1]-[5]. A conventional flat circular coils based contactless energy transmitting design was proposed for electric vehicles (EV) battery charging in [6], with introduction to inductively coupled technology. The compensation topologies have been evaluated in [7], which concluded that the series-series (SS) topology could perform the best. Among the proposed wireless energy transfer technologies, most of the studies regarded the CPT system issues as near-field transformer problems and analysed their models from equivalent circuits and electronics points of view. However, the CPT inductive coupling via air space or cores could be nonlinear scenarios due to permeability μ and B-H relations of the specific materials used within the coupling module, which causes that the mutual inductive coupling unit cannot be equivalent to a fixed electronic circuit like that of conventional ideal transformers.

In this paper, considering the changeable flux linkage and variable magnetic coupling against different operating frequencies, shielding materials and other factors in real CPT situations, the modelling and analysis based on electromagnetic field and 3D finite element methods (FEM) have

been implemented in order to evaluate the three different shielding methods using ferromagnetic materials and conductive metallic materials. From aspects of both the electromagnetics and power electronics, the flux linkage, magnetic flux density, magnetic field strength and flux line distribution in real-time field have been investigated, along with power electronics indices which are induced currents, system output RMS real power, and system power transfer efficiency and so on. By comparisons of using steel 1010, ferrite and aluminium as shielding materials for the designed small-sized CPT system, aluminium shielding appears to yield the highest overall system perform within these three shielding methods.

2. CPT system design

2.1. System overview

An electromagnetic resonant coupling based CPT system consists of AC power supply, rectifier, high frequency inverter, capacitance compensation topology, magnetic coupler, high frequency rectifier, voltage regulator and load end. In order to optimize the RMS real power transfer and efficiency of the CPT system, the design of the magnetic coupling coil modular called coupler in this paper acts as a highly significant part in the overall system when the effectiveness of a constantly satisfactory magnetic flux generation and inductive coupling tend to occur at resonant conditions in between the space of coupler coils and ferromagnetic cores. In addition to the important role of the coupler, an efficient power electronic circuit including soft switching and active rectifier devices could also highly contribute to the CPT system performance [8]-[10].

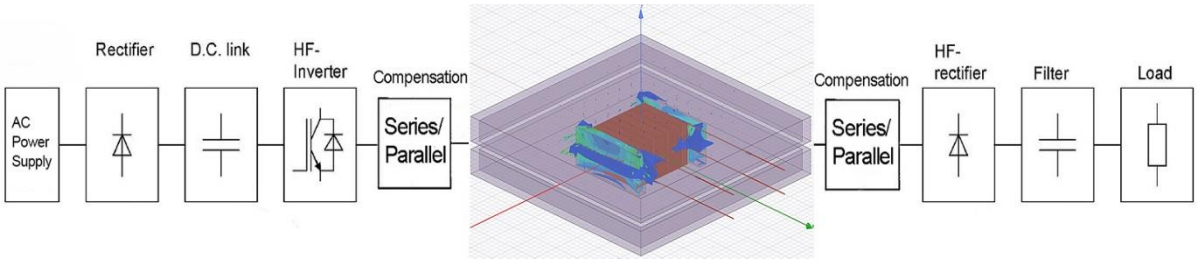

Figure 1. The H-shape coupler CPT system configuration with combined semi-enclosed shielding.

Within the space of inductive coupling, optimally shaping the flux line trajectories and forming the flux distributions using H-shape ferrite cores could expectedly improve the actual flux linkages and induced currents in real-world CPT scenarios. Practically, the high permeability and low core loss of ferrite materials could contribute to flux linkage and magnetic flux density in order for the CPT system to produce an optimized electromagnetic field performance especially when the electromagnetic resonant coupling tends to occur at specific conditions [11]. A stationary CPT system layout using the designed H-shape coupler with four compensation topologies (series-to-series, series-to-parallel, parallel-to-series and parallel-to-parallel) has been shown in figure 1. To achieve the magnetic resonance when the proposed CPT system tends to be stably operating, an appropriate capacitance compensation topology could be utilized to maximize energy transmitting capability between inductively coupled coils mounted on the designed H-shaped ferrite cores and as well as to minimize the magnitude of the real time values of reactance in the coupler. Thus the series-to-series (SS) compensation has been selected for the CPT system in this study, as shown in figure 2 below.

In order to analyse the inductive coupling performance of the proposed CPT system, based on RLC circuit theories, impedance matching principle and initial system tests with calculations for conditions of approaching electromagnetic resonant coupling, the designed system circuit parameters have been configured in figure 2, in which both the compensation capacitors are set with 150 nF, the load is set with a resistor of 50 ohm and a voltage source with an RMS value of 5 kV has been adopted as the system power supply.

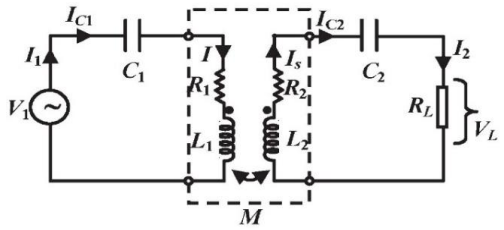

Figure 2. The simplified equivalent circuit of the CPT system with SS compensation topology.

2.2 *Geometric modeling for CPT coupler with semi-enclosed shielding*

Since the physical and geometric implementation of the coupling modular for the CPT system can definitively determine a maximum efficiency and highest transferred real power, the actual coupler design is important in the system configuration as well as considering the coupler size as one of the criteria.

To promote the magnetic flux density, flux linkage, mutual inductance and field strength, the specifically proposed H-shape core using Steel 1010 as ferromagnetic core material is designed to guide the magnetic flux along the expected paths. On the other hand, preventing energy loss in surrounding air [12] and conductive materials on the chassis of the vehicle and reducing the magnetic field flux leakage can be also contributive to the overall CPT system performance, which could be achieved by using passive magnetic shielding.

Due to the effects of high permeability and relative low eddy current loss of using ferromagnetic or conductive materials, the magnetic flux could be guided and formed by passive magnetic shielding methods [13]. Therefore, Steel1010, ferrite and aluminium have been utilized as the shielding materials in the Ansys 3D Maxwell platform based experiments in this paper. The Steel1010, as a ferromagnetic material, has nonlinear B-H curve. The ferrite adopted in this study has a relative permeability μ of 1000. The aluminium has a relative permeability μ of 1.000021.

In this paper, the H-shape coupler and the combined semi-enclosed passive shielding have been prototyped as presented in figure 3. The three different shielding materials are utilized to the CPT system coupler to output the performance results, respectively. Litz wire is selected for the windings in this model due to its skin effects reduction, proximity effects mitigation and capability for high frequency application. The small-sized magnetic coupler is designed as the geometric parameters given in table 1.

Table 1. The geometric characteristics of the H-shape coupler with passive shielding.

Parameters	Values
Winding size	100 mm x 100 mm x 20 mm
Core size	150 mm x 150 mm x 20 mm
H-shaped core bar size of each side	150 mm x 15 mm x 20 mm
Primary winding number of turns	80 turns
Secondary winding number of turns	80 turns
Air gaps of the CPT charging system	10 mm
Shielding size	400 mm x 400 x 30 mm
Shielding thickness	10 mm
Inner distance between shielding and coil	5 mm
Passive magnetic shielding materials	Steel 1010, Ferrite and Aluminium

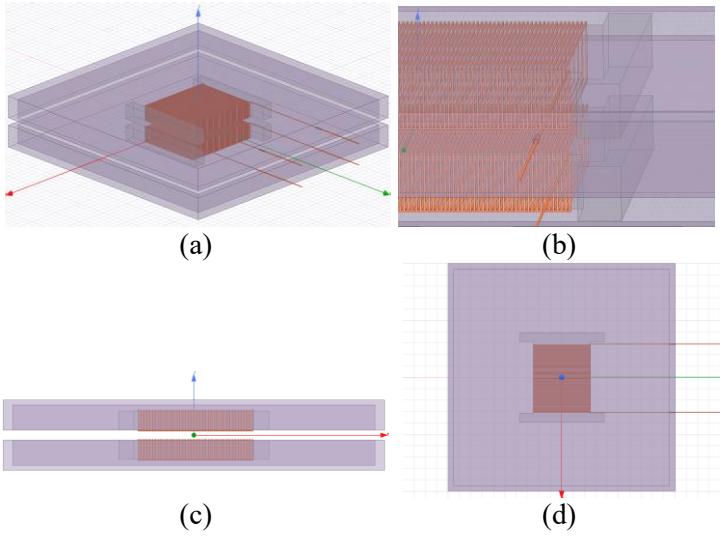

Figure 3. The H-shape coupler with the combined semi-enclosed shielding built in 3D FEM platform. (a) The CPT system coupler overview. (b) Detailed view of the windings and cores. (c) Left view of the system. (d) Top view of the system.

3. Basic principles and numerical representations of an electromagnetic resonant CPT system

To investigate and analyse the CPT system outputs with its expected electromagnetic coupling performance, the electric current density **J** induced on the secondary side of the coupler model is required to be determined. Hence, the Maxwell equations constitutively expressed by Ampere's law in equation (1), Gauss' law in equation (2), Faraday's law in equation (3) and the B-H curve relation in equation (4) are required to be solved:

$$\nabla \times \mathbf{H} = \mathbf{J} \tag{1}$$

$$\nabla \cdot \mathbf{B} = 0 \tag{2}$$

$$\nabla \times \mathbf{E} = -\frac{\partial \mathbf{B}}{\partial t} \tag{3}$$

$$\mathbf{B} = \mu \mathbf{H} \tag{4}$$

where **H** is the magnetic field strength in ampere per meter (A/m), **B** is the magnetic flux density in tesla (T), **E** is the electric field strength in volt per meter (V/m), and μ is the permeability non-linearly depending on local value of **B** in $\mathbf{B} = f(\mathbf{H})$. The electric current density **J** is in ampere per square meter (A/m^2).

$$\mathbf{B} = \nabla \times \mathbf{A} \tag{5}$$

Simultaneously with Ohm's law in electromagnetics by equation (6) and material equations of Pouillet's law by equation (7), the 3D finite-element method (FEM) is adopted to numerically solve Maxwell equations above and the relative material equations, using the methods of discretizing the modelled 3D space by tetrahedrons, translating the differential equations into algebraic equations [14]. The methods of semi-iterative conjugate gradient for each magnetic vector potential **A** [15], based on the initial B-H curve, constant values of μ can be selected for each finite element depending on local nonlinear value of **B** for the beginning. The flux density **B** values afterwards can be computed according to the calculated magnetic vector potential **A** by equation (5) derived fro*m* Gauss' law of equation (2). Repeatedly, the numerical computations can be completed until the convergence of the element permeability. It is known that

$$\mathbf{J} = \sigma \mathbf{E} \tag{6}$$

$$\mathbf{R} = \boldsymbol{\rho}\frac{\mathbf{l}}{\mathbf{C}} \tag{7}$$

where $\boldsymbol{\sigma}$ is the material-dependent parameter conductivity. $\boldsymbol{\rho}$ is the resistivity of the windings. **R** is known as electric resistance of the wire material. **l** is the total length of the wire. **C** is the cross-sectional area of the wire.

Based on the equations above, equation (1) turns into:

$$\nabla \times (\frac{1}{\mu}\nabla \times \mathbf{A}) = \mathbf{J} \tag{8}$$

$$\mathbf{E} = -\nabla\phi - \frac{\partial \mathbf{A}}{\partial \mathrm{t}} \tag{9}$$

together with Faraday's law and Lorenz gauge vector potential by equation (9) [16], by using 3D FEM computations, the magnetic flux density **B**, the electric field strength **E** and the magnetic field with values of magnetic flux ϕ in weber can be numerically solved and determined.

In order to determine the self-inductance values of **L** in henry produced by the electromagnetic field on the both sides of the CPT system, the relations between the coil current values of i and the flux linkage λ satisfy:

$$\lambda_1 = \mathrm{N}_1\phi_1 = \mathrm{L}_1 i_1 \tag{10}$$

$$\lambda_2 = \mathrm{N}_2\phi_2 = \mathrm{L}_2 i_2 \tag{11}$$

$$\mathrm{L} = \frac{\lambda}{i} \tag{12}$$

In addition, based on the RLC circuit theories [17] and circuit resonance conditions [18], the approximate natural resonant frequency for the designed coupling system in this paper can be determined in order to specify the power source operating frequencies, which then is for the analysis and optimization of the actual system performance.

To study the actual inductive magnetic coupling outcomes and electromagnetic field performance represented and reflected by the numerical vectors and scalars above, the actual RMS power generations given by equation (13) and the efficiencies given by equation (14) and (15) from the front end to the load end of the CPT system are required to be calculated, compared and analysed. cos φ is the power factor (PF) caused by phase difference φ between the induced voltage and current waveforms.

$$\mathrm{P}_{RMS} = \mathrm{V}_{RMS}\,\mathrm{I}_{RMS}\,|\cos\varphi| \tag{13}$$

$$\eta_{Coupler} = \frac{\mathrm{P}_{\mathrm{RMS}_{Secondary\ coil}}}{\mathrm{P}_{\mathrm{RMS}_{Primary\ coil}}} \tag{14}$$

$$\eta_{Overal\ system} = \frac{\mathrm{P}_{Load}}{\mathrm{P}_{\mathrm{RMS}_{Power\ supply}}} \tag{15}$$

4. Results and analysis

4.1. Flux linkage and currents with different shielding materials

In this investigation in terms of different ferromagnetic and conductive metallic shielding materials, the proposed H-shape coupler CPT system performance has been investigated across the major significant range of operating frequency and has been emphasized on the characteristic trends, from both the electromagnetics and electronics points of view. Theoretically, the flux linkage in electromagnetics and the induced current in power electronics have relatively reflective relations to the system performance based on Maxwell equations and induction principles.

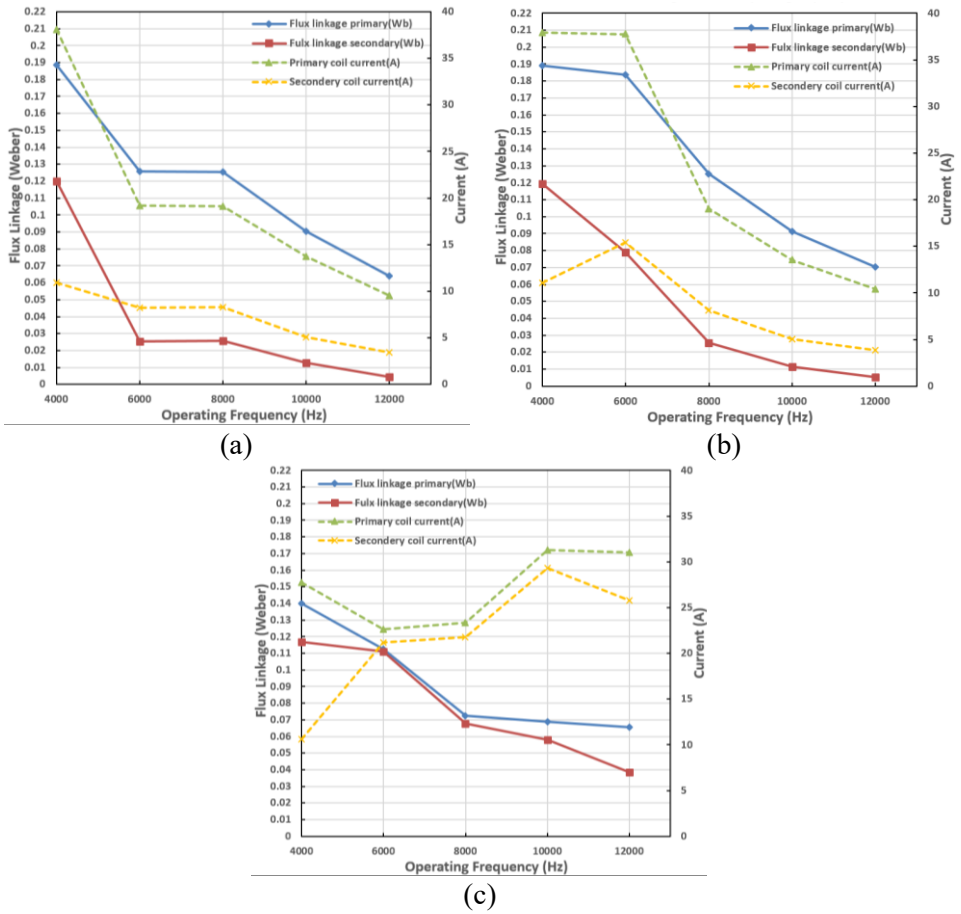

Figure 4. The flux linkage and current values of the designed CPT system versus system operating frequency. (a) Steel 1010 as shielding material. (b) Ferrite as shielding material. (c) Aluminium as shielding material.

From figures 4(a), (b) and (c), it can be seen that both the primary and secondary values of flux linkage for three shielding materials tend to decrease against the increase of system's operating frequency. Similarly, the primary and secondary coil currents for steel 1010 and ferrite in figure 4(a) and (b) show the decreasing trends. However, the values of primary and secondary coil currents tend to increase after 6000 Hz in figure 4(c), which may reflect better inductive capability of aluminium to produce satisfactory coupling for the system than steel 1010 and ferrite as passive shielding material.

In terms of the characteristic values, the flux linkage of primary and secondary coils for steel 1010 have shown relatively stable values of about 0.1257 Wb and 0.0258 Wb, respectively, corresponding to frequency range of 6000 to 8000 Hz in figure 4(a), after which these two values gradually tend to decrease. In the meantime, the induced currents of primary and secondary coils have the similar tendency like the corresponding flux linkages. It could be noticed that the values of primary and secondary currents tend to stabilize at about 19.13 A and 8.25 A, respectively, when the system operating frequency is supplied between 6000 Hz to 8000 Hz, in figure 4(a).

Regarding the flux linkage and current values for ferrite shielding in figure 4(b), both the values of the flux linkage of primary and secondary sides have a gradually moderating trend from 0.1890 Wb and 0.1195 Wb at 4000 Hz, respectively, down to 0.0703 Wb and 0.0054 Wb at 12000 Hz. While the primary coil current shows stable trend before 6000 Hz, after which a sharp drop can be seen against the operating frequency. However, the secondary coil current shows a peak value of 15.39 A at 6000 Hz, which is also the calculated optimal resonant coupling point for ferrite as shielding material.

With regard to shielding using conductive metallic material, aluminum shielding for the designed CPT system can be initially seen as a proper shielding method according to figure 4(c). The overall values of primary and secondary flux linkage are higher than steel1010 and ferrite despite the similar downward tendency. It could be seen that, after 8000 Hz, flux linkage values of primary and secondary sides show gradually decreasing change until 0.0581 Wb and 0.0384 Wb, respectively, at 12000 Hz, which is higher than the final and lowest values of steel 1010 and ferrite.

4.2. RMS real powers and efficiencies with different shielding materials

As indispensable indices for evaluating the CPT system performance, the RMS real power and efficiency across a range of system operating frequency could reflect the design effectiveness for the energy transmitting purpose of a system in real-world applications. In this paper regarding the three different shielding materials, the actual values of real transferred power and efficiency on both coil sides of the designed coupler are compared and analyzed.

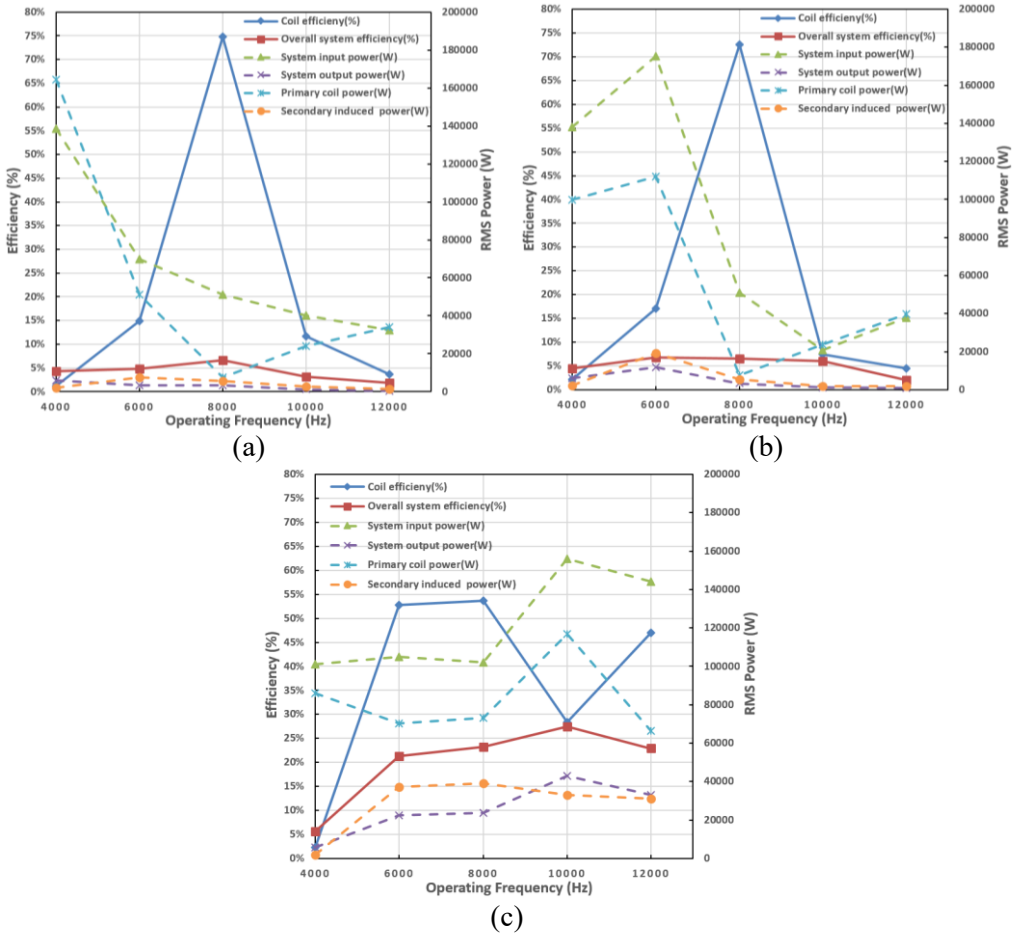

Figure 5. The RMS real powers and efficiencies of the designed CPT system versus system operating frequency. (a) Steel1010 as shielding material. (b) Ferrite as shielding material. (c) Aluminium as shielding material.

The actual electromagnetic field parameters generated are variable and the real-time phase angle differences are changeable in terms of various system operating frequencies [11], as well as the different shielding materials proposed in this paper, which determines the RMS real power and efficiency. Based on the actual power factor (PF) generated and original waveforms acquired after the CPT system outcomes stabilize at each testing operating frequency, the resulted values of RMS real power and efficiency can be worked out and analyzed.

From figure 5(a), it can be seen that the coil energy transfer efficiency could reach a peak value of 74.76% at 8000 Hz, at which point the system efficiency also reaches a maximum of 6.67%. The system input power significantly drops from 138.62 kW to 32.51 kW while the system output power on the load also reduces by about 10 times from 5.92 kW to 0.59 kW. It is noticeable that the primary coil power decreases to a lowest value of 7.51 kW at 8000 Hz whilst the secondary coil power could produce a second highest value on its curve, which causes the peak values 74.76% and 6.67%, respectively, for the coil efficiency and system efficiency.

Figure 5(b) depicts almost the same trend for the coil efficiency like in figure 5(a), whilst the overall system efficiency show a stably higher range of values over 6% across the operating frequency range between 6000 Hz to 10000 Hz. The overall system efficiency reaches its maximum of 6.77% at 6000 Hz. Importantly, it can be noticeably seen that the system input power, system output power on load, primary coil power and secondary coil achieve their maximum values of 175.19 kW, 11.85 kW, 112.11 kW and 19.11 kW, respectively, at the calculated magnetic resonant coupling frequency of about 6000 Hz.

Regarding the performance of aluminium shielding, it can be noticed that almost all the results of the system could show improvements in figure 5(c). Significantly, the overall system efficiency could reach a peak value of 27.48% at 10000 Hz and could also stay at stably satisfactory values of over 20% when the operating frequency is supplied with 6000 Hz and above. The system output power on load end achieves a maximum of 42.90 kW at 10000 Hz.

Therefore, the aluminium shielding performs with the highest results of criteria within the three shielding materials, which indicates satisfactory power transfer rating, efficiency in addition to acceptable electromagnetic field flux distributions and coupling performance.

4.3. Analysis and comparison on main results with different shielding materials based on electric vehicle charging

In addition to graphic trend analysis for each model with different shielding methods above, table 2 below could indicate the major critical results for comparing and evaluating the CPT system outcomes and performance. As known, the load current could firstly reflect the effectiveness of inductive coupling phenomena, by which it can been seen that the CPT system with aluminium could produce highly effective inductive coupling for electric vehicle contactless charging applications than systems with steel 1010 and ferrite shielding according to numerical comparisons in table 2.

Generally, electric vehicles (EV) could gain faster charging depending on higher CPT system output real power rating. From table 2, the system output power of steel1010 shielding is unable to deliver a rating value of over 1 kW, while the ferrite shielding CPT system can produce 11.85-kW system output power on load at its resonant coupling status with the calculated natural resonant frequency of about 6000 Hz. Noticeably, the CPT system with aluminium shielding could generate relatively high system output real power across a wider range of operating frequency, which contributes to a maximum value of 42.90 kW when the CPT system performs to stabilize, at the resonant coupling frequency of about 10000 Hz. When considering the energy use efficiency from the power supply, the overall system efficiency could be of reference. By comparison, the aluminium shielding CPT system is able to produce relatively high system efficiency especially at 10000 Hz as presented in table 2.

Table 2. Main numerical results of the H-shape coupler CPT system with threes passive shielding materials.

Operating Frequency (Hz)	CPT system with Steel1010 Shielding			CPT system with Ferrite Shielding			CPT system with Aluminium Shielding		
	Load Current (A)	System Output Power (W)	Overall System Efficiency	Load Current (A)	System Output Power(W)	Overall System Efficiency	Load Current (A)	System Output Power (W)	Overall System Efficiency
4000	10.8830	5921.6438	4.2718%	11.0816	6140.1916	4.4533%	10.6396	5659.8033	5.6023%
6000	8.2543	3406.8649	4.8806%	15.3962	11852.4135	6.7656%	21.1614	22389.6902	21.3399%
8000	8.2598	3411.4717	6.6690%	8.1282	3303.6662	6.4895%	21.7739	23704.4088	23.2055%
10000	5.0780	1244.7123	3.0932%	5.0251	1262.4810	6.0493%	29.2918	42899.5869	27.4804%
12000	3.4414	593.2719	1.8249%	3.8790	752.3685	1.9919%	25.8064	33008.5921	22.9075%

4.4. Analysis on a selected CPT system model with aluminum shielding method based on electromagnetic field

Based on comparisons and analysis in previous sections, it can be found that the H-shape coupler CPT system with aluminium shielding could provide highest power electronic performance in the three shielding methods. Thus, the CPT system with aluminium shielding, at its optimal performance frequency of 10000 Hz, has been selected to be analysed from aspects of the electromagnetics.

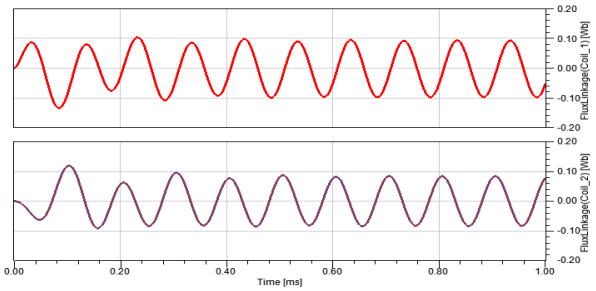

Figure 6. The flux linkage waveforms of the designed H-shape coupler CPT system with aluminium passive shielding, at the operating frequency of 10000 Hz.

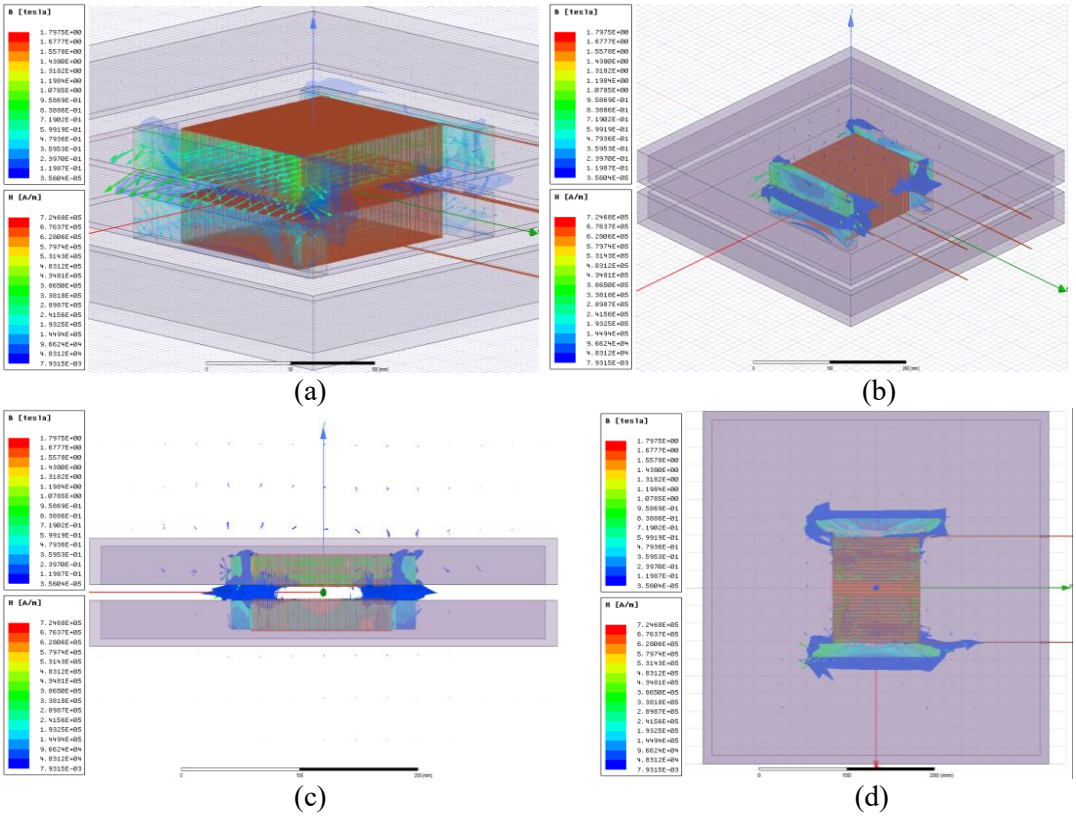

Figure 7. The electromagnetic field of the designed H-shape coupler CPT system with aluminium passive shielding at 1 *m*s, indicating the magnetic field strength **H** and the magnetic flux density **B**, at 10000 Hz. (a) The **B** vector in the field. (b) The dimitric view of the field. (c) The left view of the field. (d) The top view of the field.

As can be seen from figure 6, the alternating flux linkage waveforms of the primary and secondary coils are able to be sinusoidally stable since the sixth period, which means the CPT system could tend to perform immediately with electromagnetic coupling stability within 1 *m*s after the system is activated to be magnetically coupled. Once the electromagnetic stability is established, the RMS

values of the primary and secondary flux linkage could be 0.0689 Wb and 0.0581 Wb, corresponding to the measured amplitude values of 0.0974 Wb and 0.0822 Wb, respectively. Besides, it also could be computed that the phase difference between the two AC flux linkages tends to be about 108 degrees when the system reaches an AC stable and magnetic resonant coupling.

In terms of the electromagnetic field parameters and performance, the CPT system with aluminium shielding at the operating frequency of 10000 Hz has been selected to be investigated as a typical magnetic resonant coupling scenario. As shown in figure 7(a), the vector arrows of the magnetic flux density **B** show the expected directions, mostly concentrating at the external edges and corners of the designed H-shaped core, along with maximum scalar magnitude of 1.7975 Teslas, In the meantime, the magnetic field strength **H** reaches its peak value of 7.2468 x 10^5 A/m at the ending point of the external corners of the core, which also indicates the effectiveness of the geometric H-shape design for shaping and guiding the flux lines.

According to figures 7(b), (c) and (d), the vector field **B** and **H** are established to be alternatively varying within the combined semi-enclosed air space by the effects of aluminium passive magnetic shielding, which can prove that the shielding does prevent the magnetic field flux distributions from spreading and leaking to the remote surrounding space. In real-world applications, this effect may consequently reduce energy losses to the air, to the surrounding conductive elements of electric vehicle chassis or even to the human driver as a potential EMI issue when in a high frequency range.

5. Discussion

As demonstrated and illustrated in the electromagnetic field of the designed H-shape coupler CPT system, the ferromagnetic material as the core with high permeability and H-shape can produce and form the magnetic flux distribution as expected, especially facilitating the magnetic flux density and magnitude field strength at the external corners and edges of the H-shape core. The optimally guided and formed flux vector trajectories and field distribution can be utilized and has been proved to promote the CPT system coupling performance from perspectives of electromagnetics.

By comparing the obtained power transfer ratings and system efficiency values of three shielding methods using different ferromagnetic and conductive materials, it can be found that deploying aluminium as shielding material could output relatively more satisfactory CPT system performance. The H-shape coupler CPT system using aluminium shielding enables to deliver a maximum overall system output RMS real power of 42.90 kW and to produce a peak system efficiency of 27.48% at about the natural resonant frequency of 10000 Hz. Besides, at higher range of operating frequencies, the CPT system with aluminium shielding appears to generate sustainable satisfactory system efficiency, transfer power rating on load and flux linkage, which could be of advantage for real-world electric vehicle contactless charging applications.

With regard to limitations, the distance between the windings and inner shielding surfaces in this prototype may be too small, which would probably have caused the ultimately optimal magnetic field flux distribution and flux linkage values to be restricted to be achieved, to some degree. In the further investigations, the distance between the windings and inner shielding surfaces is supposed to be enlarged from 5 mm to 15 mm under the preconditions of expected shielding functions and limited space usage, to find out the optimized inner shielding distance for the CPT system.

In real-world applications, the actual electromagnetic field performance and inductive coupling quality can be significantly affected by how the electric vehicle is parked over the ground side power transmitting module with longitudinal and lateral misalignments, which should be counted as system tolerance to parking misalignment. In addition, the module size of CPT system will have to be optimized to be completely suitable to real-world vehicle chassis for installation and application.

6. Conclusion

In this paper, a small-sized geometrically improved H-shape coupler CPT system and the basic principles of electromagnetic resonant coupling model have been presented, along with the analysis and discussion on RMS power transfers, CPT system efficiencies, generated electromagnetic field

characteristics and performances of using three passive shielding materials. It can be found that the magnetic field flux distributions have been optimally formed by the designed ferromagnetic H-shape core. By using aluminium passive shielding to facilitate the field flux paths, the CPT system could output a maximum overall system efficiency of 27.48% and a peak RMS real power of 42.90 kW on the system load end, at about 10000-Hz operating frequency when the CPT system tends to perform with magnetic resonant coupling status. In addition, the limitations of the designed CPT system and some future focuses have been discussed.

References

[1] Budhia, M., Vyatkin, V. & Covic, G.A., 2008. Powering flexible manufacturing systems with intelligent contact-less power transfer. *2008 6th IEEE International Conference on Industrial Informatics*, pp.1160–1165.
[2] Pengfei Li, R. & Bashirullah, 2007. A Wireless Power Interface for Rechargeable Battery Operated Medical Implants. *IEEE Transactions on Circuits and Systems II: Express Briefs*, 54(10), pp.912–916.
[3] Radecki, A. et al., 2011. 6W/25mm2 inductive power transfer for non-contact wafer-level testing. *2011 IEEE International Solid-State Circuits Conference*, pp.230–232.
[4] Kurs, A. et al., 2007. Wireless power transfer via strongly coupled magnetic resonances. *Science (New York, N.Y.)*, 317(5834), pp.83–86.
[5] Hui, S.Y.R. & Ho, W.W.C., 2005. A new generation of universal contactless Battery Charging platform for portable Consumer Electronic equipment. *IEEE Transactions on Power Electronics*, 20(3), pp.620–627.
[6] Chwei-Sen Wang, O., Stielau & Covic, 2005. Design considerations for a contactless electric vehicle battery charger. *IEEE Transactions on Industrial Electronics*, 52(5), pp.1308–1314.
[7] Villa, J.L. et al., 2012. High-Misalignment Tolerant Compensation Topology for ICPT Systems. *IEEE Transactions on Industrial Electronics*, 59(2), pp.945–951.
[8] Hosotani, T. & Awai, I., 2012. A novel analysis of ZVS wireless power transfer system using coupled resonators. *2012 IEEE MTT-S International Microwave Workshop Series on Innovative Wireless Power Transmission: Technologies, Systems, and Applications*, pp.235–238.
[9] Yang Sun et al., 2011. A high speed comparator based active rectifier for wireless power transfer systems. *2011 IEEE MTT-S International Microwave Workshop Series on Intelligent Radio for Future Personal Terminals*, pp.1–2.
[10] Kim, S. et al., 2010. Semi-active high-efficient CMOS rectifier for wireless power transmission. *2010 IEEE Radio Frequency Integrated Circuits Symposium*, pp.97–100.
[11] Duan, J. & Wang, W., 2018. Electromagnetic Coupling Optimization by Coil Design Improvements for Contactless Power Transfer of Electric Vehicles. In Proceedings of the Future Technologies Conference (FTC) 2018. *Advances in Intelligent Systems and Computing*, vol 881, pp. 944-958.
[12] Paul, C.R., 1992. *Introduction to electromagnetic compatibility*, New York: Wiley.
[13] Wohlfarth, E. P., 1982. *Ferromagnetic Materials: A Handbook on the Properties of Magnetically Ordered Substances*. Amsterdam: North-Holland.
[14] Sadiku, M., 1992. *Numerical techniques in electromagnetics*, Boca Raton: CRC P.
[15] Silvester, P., Ferrari, R., 1990. *Finite elements for electrical engineers* 2nd ed., C.U.P.
[16] Jackson, J.D. & Okun, L.B., 2000. Historical roots of gauge invariance. *Reviews of Modern Physics*, 73(3), pp.663–680.
[17] Grover, F., 1962. *Inductance Calculations: Working Formulas and Tables*. Dover.
[18] Rashid, M.H., 2004. *Power Electronics: circuits, devices, and applications* 3rd ed., Upper Saddle River, N.J.: Prentice Hall.